Assessing the differences in net primary productivity between pre- and post-urban land development in China

Fengsong Pei, Xia Li*, Xiaoping Liu, Shujie Wang, Zhijian He

Guangdong Key Laboratory for Urbanization and Geo-simulation, School of Geography and Planning, Sun Yat-sen University, Guangzhou 510275, PR China

ABSTRACT

Urban land development substantially alters the terrestrial carbon cycle, particularly the net primary productivity (NPP), from local to global scales. However, limited attempts have been undertaken to elucidate the differences in NPP between pre- and post-urban land development in China. In this paper, the terrestrial NPP after urbanization in China was assessed by using the Carnegie-Ames-Stanford approach (CASA), toward which a calibration was conducted for adapting this model on the fine-scale application. In addition, a method of neighborhood proxy was applied to acquire the NPP in the absence of urban land development, assuming that non-urban lands can represent their nearby urban lands before they were transformed. Our analyses indicate that urban land development had overall negative effects on terrestrial NPP. They reduced the NPP at an accelerating rate of 0.31×10^{-3} Pg C year^{-1}, approximately 5.88% of the annual reduction during the period of 2000–2006 in China. Furthermore, these effects of NPP variations exhibited obvious differences in the amounts and spatial distributions. However, the NPP showed a slight increase around some regions that experienced rapid urbanization, as well as the arid regions in northwest China. These were probably caused by the effects of Urban Heat Island (UHI) and Urban Rain Island (URI), an introduction of faster growing exotics, various resource augmentations and so on.

© 2012 Elsevier B.V. All rights reserved.

1. Introduction

Land-use/cover change (LUCC) induced by human activities dramatically alters the processes and functions of natural ecosystems, as well as the services they provide, from local to global scales (Alberti, 2005; Buyantuyev and Wu, 2009). Both tropical deforestation and temperate cultivation have been widely investigated to understand their effects on the processes of global carbon cycle (DeFries et al., 2002; Huang and Sun, 2006). However, urban land development, another type of land-use change, which is also worldwide prevalent, has not been well studied by researchers in global climate change analysis (Kaye et al., 2005). Despite the occurrence on less than 3% of global land surface, urban land development exhibits remarkable effects at a global scale, being responsible for 78% of carbon emissions, 60% of residential water use and so on (Grimm et al., 2008). This phenomenon not only substantially transforms the landscapes, but also alters the biogeochemical cycle and photosynthetic productivity of terrestrial ecosystems (Gregg et al.,

2003; Buyantuyev and Wu, 2009). Thus, it is meaningful to explore the effects of urban land development on the carbon cycle, and the adaptive mechanisms of the terrestrial ecosystems in response to global changes. However, there are limited attempts to address such problems, especially in the rapidly urbanized regions (Milesi et al., 2003).

Numerous issues concerning the consequences of urban land development on carbon cycle can be addressed, including net primary productivity (NPP) and net ecosystem productivity (NBP). However, this paper concentrates specifically on how urban land development affects the terrestrial NPP. The NPP pertains to a production of organic compounds, principally through a process of photosynthetic production. During the past decades, increasing studies regarding the effects of urban land development on NPP have been conducted at different scales. At a national scale, consequences of urban land transformation in the United States were examined by using data from two satellites and a terrestrial carbon model (Imhoff et al., 2004). They found that urbanization had large negative impacts on NPP. Additionally, Milesi et al. (2003) investigated the effects of urban land development in the southeastern United States on regional NPP through a combination of MODIS data, DMSP-OLS nighttime light data and Landsat ETM images. At a city scale, a comparison of the NPP was performed between natural and anthropogenic land covers in the Phoenix metropolitan region of the USA (Buyantuyev and Wu, 2009). Their findings

* Corresponding author at: School of Geography and Planning, Sun Yat-sen University, 135 West Xingang Rd., Guangzhou 510275, PR China.
Tel.: +86 13924203023; fax: +86 020 84115833.
E-mail addresses: lixia@mail.sysu.edu.cn, lixia@graduate.hku.hk (X. Li).
URL: http://www.geosimulation.cn/ (X. Li).

revealed that urban land development might boost productivity by introducing highly productive plant communities and weakening the coupling of plant growth to the naturally occurring cycles of water and nutrients in arid environments. In terms of China, Xu et al. (2007) evaluated the effects of urbanization on NPP in Jiangyin County between 1991 and 2002 by using satellite images and a boreal ecosystem productivity simulator model. Yu et al. (2009) took Shenzhen City as a typical case and estimated the influences of urban sprawl on NPP. However, limited attempts have been made to understand the differences in NPP caused by the urban land development in China. There is a general lack on the studies of the regional patterns and the causes of the differences for this whole country. In addition, NPP is primarily dominated by solar radiation, precipitation, temperature, nitrogen limits, ambient CO_2 concentration, land covers and other local environmental factors simultaneously and interactively (Cramer et al., 1999; Wang and Houlton, 2009). It is a difficult task to distinguish the contributions of these influencing factors to the variations of NPP. Especially, the methods to isolate the contributions of urban land development from that of climate change to the NPP variations have not been well explored because of their complexities (Xu et al., 2007; Lu et al., 2010).

While modeling the NPP, a wide range of models have been developed (Potter et al., 1993; Cramer et al., 1999). Among these models, the CASA has been well employed in assessing the terrestrial NPP in United States (Lobell et al., 2002), in China (Piao et al., 2005), as well as at a global scale (Potter et al., 1993). Maximum light use efficiency (ε_{max}) is considered to be a key parameter influencing the NPP calculations of the CASA (Piao et al., 2001; Zhu et al., 2006). Researchers have developed various methods to determine this factor. For instance, photochemical reflectance index (PRI), which based on the reflectance at 531 and 570 nm, proved to be effective in deriving the light use efficiency (ε) by using both ground spectral measurements and satellite observations (Nichol et al., 2000; Inoue and Peñuelas, 2006; Goerner et al., 2011). However, PRI showed high sensitivity to various extraneous effects such as canopy structure and view observer geometry (Wu et al., 2010; Hilker et al., 2010). In addition, ε_{max} varies with vegetation types, spatial scales and the uniformity of vegetation coverage. There are still many uncertainties in the value of this parameter. Russell et al. (1989) proposed that ε_{max} varies in the range of 1.1–1.4 g C MJ^{-1} for croplands. Potter et al. (1993) set ε_{max} to be 0.389 g C MJ^{-1} for all types of global vegetation via a single calibration by using AVHRR Normalized Difference Vegetation Index (NDVI) satellite data at a resolution of 1 × 1 degree. Zhu et al. (2006) simulated ε_{max} for several typical vegetation types in China by applying an algorithm of modified least squares function based on the AVHRR NDVI satellite images at 8-km resolution. Propastin et al. (2012) simulated ε by using the SeaWiFS NDVI at a resolution of 4.63 km^2. However, the satellite data at a low resolution limits the applicability of their simulated parameter ε_{max} to investigate the effects on carbon cycle of such fine-scale phenomenon as urban land development.

This paper investigates the temporal and spatial distributions of the NPP in China, together with the dynamics of the NPP from the pre- to post-urbanization through a combination of satellite images, forest inventory data and corresponding ground-based information. One of light use efficiency models, the CASA, was employed to estimate the terrestrial NPP after urbanization in China. A calibration was performed to obtain ε_{max} for the fine-scale application of this model by using 1-km MODIS NDVI. While assessing the terrestrial NPP before urbanization, we attempted to apply a method of neighborhood proxy to separate the contributions of urban land development from other factors such as temperature, precipitation and so on. Consequently, the effects of urban land development on NPP in China were evaluated, and some

analyses were carried out based on vegetation types, dry-wet zones and so on.

2. Data and preprocessing

2.1. Measurement-based biomass and NPP data

The field-based forest biomass/NPP data, which were widely used in previous studies (Ni, 2003; Feng et al., 2007), were derived according to Luo (1996)'s study. The data were mainly compiled based on the national forest inventories conducted by the Chinese ministry of forestry during 1989–1993, and some other published literatures from some intensively studied and well-documented field sites. In addition, the forest biomass and NPP data consist of many site-dependent records such as the biomass and NPP for most of the plant components including stem, branch, leaf, root, as well as the entire ecosystems. Some other literatures such as latitude, longitude, elevation, dominant species, stand age, density, volume, leaf area index, are available as well. The biomass and NPP data for grassland and shrubland were obtained from several published works (Jin et al., 2007; Ni, 2004; Togtohyn and Ojima, 1996; Wang et al., 2011; Yu et al., 2000). These were selected because: (1) a series of measurements were made at intervals during the growing season within one year or more; (2) the data on aboveground and belowground biomass were available. As a result, the values of corresponding NPP were calculated by using the method of Ni (2003) based on the maximum and minimum biomass. Most of the biomass and NPP records were provided in the unit of dry matter (DM). Thus, a conversion was performed from DM to carbon content (g C m^{-2} year^{-1}) by applying a conversion factor of 0.5 for woody biomass (Myneni et al., 2001), and 0.45 for grassland and shrubland (Fang et al., 2007).

2.2. Climate datasets from NMIC/CMA and GES DISC

The climate dataset employed in this work, which covers the period of 2000–2010, includes monthly mean temperature, total monthly precipitation and monthly solar radiation across China. Specifically, some historical records of monthly temperature and precipitation were derived from 752 climatological stations in China. Monthly solar radiation data were compiled from 122 solar radiation observation stations. All these data were provided by the Chinese National Metrological Information Center/China Meteorological Administration (NMIC/CMA). For assuring the continuity and consistency, we validated these data by screening and eliminating the suspicious and missing records. In addition, the spatial distributions of these factors are required by the CASA model. As an important interpolation method, kriging has been widely used when regionalizing various variables at different scales (Piao et al., 2001; Zhu et al., 2006). Thus, in terms of the climate factors from the site-based information, a spatial interpolation of kriging was applied for each station at a resolution of 0.01 × 0.01 degree. In addition, the data on Tropical Rainfall Measuring Mission (TRMM) rainfall product (3B43) from 2001 to 2010 were obtained from Goddard Earth Sciences Data and Information Services Center (GES DISC). The TRMM 3B43 data were then averaged for each month of the 10-year period. Annual total rainfall for each cell was calculated based on 3B43's monthly precipitation rate (mm h^{-1}). As a matter of convenience, these images were resampled from a resolution of 0.25 × 0.25 degree to 0.01 × 0.01 degree as well, although this did not increase the effective resolution of the data.

2.3. NDVI and LST data from MODIS

The development of MODIS sensor marked the beginning of a new era in the remote sensing of the earth for its medium

Table 1
Maximum light use efficiency ($\varepsilon_{\max}$) of the typical vegetation types in China. ENF, evergreen needleleaf forest; EBF, evergreen broadleaf forest; DNF, deciduous needleleaf forest; DBF, deciduous broadleaf forest; NBMF, needleleaf-broadleaf mixed forest; DBMF, evergreen-deciduous broadleaf mixed forest; UL, urban lands; Others, the barren or sparsely vegetation.

Vegetation types	$\varepsilon_{\max}$ (g C MJ^{-1})	Vegetation types	$\varepsilon_{\max}$ (g C MJ^{-1})
ENF	0.366	Shrub	0.348
EBF	0.630	Grass	0.421
DNF	0.383	Crop	0.421
DBF	0.478	UL	0.421
NBMF	0.446	Others	0.421
DBMF	0.547		

spatial, high spectral and temporal resolutions. In this paper, the NDVI images, which cover the period 2001–2010 at a spatial resolution of 1 km^2, were derived from the MODIS monthly NDVI product (MOD13A3). The 8-day land surface temperature (LST) data with the same resolution as NDVI in December for the period 2001–2010 in China were also obtained from MODIS LST product (MOD11A2). These images were downloaded from the EOS Data Gateway at the Land Processes Distributed Archive Center (https://lpdaac.usgs.gov/products/modis_products_table), a part of NASA's Earth Observing System Data and Information System. These data were then aggregated to geographic grid cells at a resolution of 0.01 × 0.01 degree from their original sinusoidal projection by using the MODIS reprojection tool (MRT). For examining the spatial distributions of Urban Heat Island (UHI) during the past decade, the LST data from 2001 to 2010 were averaged to represent the stable heat distributions in this period.

2.4. Vegetation map and soil texture data

The spatial distributions of various types of vegetation in China were generated from a vegetation map at a scale of 1:1,000,000 (Editorial Board of Vegetation Map of China, 2001), which was primarily derived from ground observations. For driving the CASA model properly, the original categories of these vegetation types were reclassified into 10 classes (Table 1, except for urban lands) according to Potter et al. (1993)'s schema.

In addition, the soil rooting depths for forest vegetation types were set to 2.0 m, and the others were assigned a rooting depth of 1.0 m (Potter et al., 1993). Soil texture is also important in determining the soil water content, and therefore the NPP. The harmonized world soil database (HWSD), which was developed by the food and agriculture organization of the United Nations (Freddy et al., 2008), shows some soil parameters for top- and subsoil, including the fraction of sand/silt/clay, soil organic carbon and so on. The soil texture classes and associated particle sizes in this study were compiled from the subset of HWSD that covers the whole China at a scale of 1:1,000,000. All these data were then aggregated to grid cells at a resolution of 0.01 × 0.01 degree.

2.5. Land use/cover from Landsat TM/ETM+

During the past decades, urban lands in China have increasingly expanded and encroached upon many arable lands (Li, 1998; Weng, 2002). For representing the land use/cover changes in China, two land use/cover datasets that cover the years 2000 and 2006 were employed in this study. The land use/cover dataset in 2000 across China were obtained from a land use dataset at a scale of 1:100,000, which were interpreted based on 512 scenes of Landsat TM/ETM+ images in 1999/2000 (Liu et al., 2005). In addition, the land use/cover data in 2006 were derived from the updating survey of land use/cover by each province in China according to Jing (2009) and Liu et al. (2005)'s methods. All these data were resampled to a resolution of 0.01 × 0.01 degree as well. Urban lands in China were then extracted from these data by using GIS. However, the

classification of these two land use/cover data toward natural vegetation does not suit the parameters and structure of the CASA model. Thus, the distributions of vegetation from the vegetation map above were used as the original natural vegetation instead.

3. Methods

3.1. The CASA model

3.1.1. Description of the CASA model

In this paper, we assessed the NPP in China by using the CASA, which was developed based on the concept of light use efficiency (Monteith, 1972; Potter et al., 1993). This model can be implemented by using NDVI, temperature, precipitation, solar radiation, land use/covers and soil texture as input. In detail, the NPP is calculated as the product of the amount of photosynthetic active radiation absorbed by green vegetation (APAR) (MJ m^{-2}) and the light use efficiency (ε) (gC MJ^{-1}) by which that radiation is converted to plant biomass increment:

$$\text{NPP}(x, t) = \text{APAR} \times \varepsilon \tag{1}$$

where NPP(x, t) (gC m^{-2}) is the net primary productivity fixed by vegetation at a grid cell x in month t, and APAR is the amount of photosynthetic active radiation.

APAR is calculated by using the data on solar surface irradiance S (MJ m^{-2}) and the fraction of photosynthetic active radiation absorbed by green vegetation FPAR. The factor ε for each grid cell can be determined as the product of $\varepsilon_{\max}$ (g C MJ^{-1}) determined by a calibration with field data, and scalars representing the availability of soil moisture W and the suitability of temperature (T_1, T_2). Thus, the NPP in location x and time t becomes:

$$\text{NPP}(x, t) = S(x, t) \times \text{FPAR} \times 0.5 \times \varepsilon^* \times T_1(x, t) \times T_2(x, t) \times W(x, t) \tag{2}$$

where the factor 0.5 accounts for the fact that approximately half of the incoming solar radiation is in the photosynthetic active radiation waveband (0.4–0.7 μm) (Potter et al., 1993). The FPAR is defined as a linear function of the NDVI simple ratio SR,

$$\text{FPAR}(x, t) = min\left[\frac{\text{SR}(x, t) - \text{SR}_{\min}}{\text{SR}_{\max} - \text{SR}_{\min}}, 0.95\right] \tag{3}$$

$$\text{SR}(x, t) = \frac{[1 + \text{NDVI}(x, t)]}{[1 - \text{NDVI}(x, t)]} \tag{4}$$

where SR$_{\min}$ refers to the factor SR for unvegetated land areas, and SR$_{\max}$ approximates the values of SR when all downwelling solar radiation is intercepted. These two factors are determined according to the schema in Potter et al. (1993)'s study.

Additionally, the effect of temperature stresses is regulated by the monthly mean temperature (T) (°C) and the temperature when NDVI reaches its maximum in the whole year (T_{opt}) (°C). The temperature factors T_1 and T_2 are calculated as:

$$T_1(x, t) = 0.8 + 0.02 \times T_{opt}(x) - 0.0005 \times T_{opt}(x) \times T_{opt}(x) \tag{5}$$

$$T_2(x, t) = \frac{1.1814}{\{1 + e^{[0.2(T_{opt}(x) - 10 - T(x,t))]}\}/\{1 + e^{[0.3(-T_{opt}(x) - 10 + T(x,t))]}\}} \tag{6}$$

The moisture stress factor (W) is determined based on the monthly averaged climate data and the corresponding soil properties:

$$W(x, t) = 0.5 + \frac{0.5\text{EET}(x, t)}{\text{PET}(x, t)} \tag{7}$$

where EET (mm) is derived from a one-layer bucket soil moisture model (Potter et al., 1993), and PET (mm) is calculated with the method of Thornthwait (1948). The details of the CASA model can be found in the studies by Potter et al. (1993).

3.1.2. Calibration of the CASA model

Given the coarse resolutions of satellite data that most studies used, a new calibration of the CASA model was performed to obtain ε_{max} by using the 1-km MODIS NDVI data. This calibration was implemented for various typical land use/covers in China (Table 1). As to one of the land use/covers, the errors between observed NPP and simulated NPP can be expressed as:

$$E(x) = \sum_{i=1}^{j} (m_i - n_i x)^2 \tag{8}$$

where i is the samples of a vegetation type; j is the number of samples of a vegetation type; m represents the observed NPP values; n is the products of APAR, T_1, T_2 and W, x is an unknown variable representing the maximum light use efficiency that needs to be simulated. By expanding Eq. (8), $E(x)$ becomes:

$$E(x) = \sum_{i=1}^{j} n_i^2 x^2 - 2\sum_{i=1}^{j} m_i n_i x + \sum_{i=1}^{j} m_i^2 \tag{9}$$

A detailed description of the steps required to do the calibration can be found in Field et al. (1995) and Zhu et al. (2006). The values of ε_{max} for forest types, shrub and grassland were calculated according to Eqs. (8) and (9). However, urban lands in this study were assumed to be one of sparse "vegetation types" such as grasslands (Zhu et al., 2006; Trusilova and Churkina, 2008), so are the croplands and the other land covers. In other words, these land use/covers were all supposed to have the same ε_{max} as grassland.

3.2. Simulation strategies for the impacts of urban land development on NPP

For exploring the effects of urban land development on NPP in China, the amounts and spatial distributions of urban lands were firstly extracted based on the land use/cover data that were compiled from the vegetation map and Landsat TM/ETM+ images. The conversion proportions of urban areas from various original land use/covers were calculated by using the vegetation map and urban land-use data. POST-U2006 NPP, PRE-U2000 NPP and PRE-UNOU NPP were then calculated as follows.

3.2.1. Average annual NPP as the POST-U2006 NPP

Post-urban conditions refer to the mean states during a period after urbanization concerning the conditions of land use, climate and so on. While deriving the post-urban NPP in China, the meteorological data during a 10-year period (2001–2010) were used, with the assumption that these records might reflect current climate conditions well. In this paper, the post-urban NPP, namely POST-U2006 NPP (NPP$_{POST-U2006}$), represents the NPP distributions based on the land use/covers in 2006 (thus maximum light use efficiency) under current climate conditions. That is, monthly and annual NPP values during a 10-year period (2001–2010) were calculated by using the CASA model based on the maximum light use efficiency, which were calibrated with the land use/covers in 2006. After that, the spatial distributions of average annual NPP during this period across China were mapped for representing the POST-U2006 NPP under current climate conditions.

3.2.2. A method of neighborhood proxy for the calculations of PRE-NOU and PRE-U2000 NPP

Pre-urban conditions reflect the distributions of the original vegetation without urban land development. Given that meteorological conditions vary from time to time, the temporal effects on NPP of a special disturbance such as urban land development are different even at same site. These effects depends on the seasonal or interannual variations of the climate conditions during the period when the disturbance occurred. For eliminating the effects of climate factors, the pre-urban NPP was computed by using a method of neighborhood proxy. This method assumes that non-urban lands could represent the best proxy to what the nearby urban lands once were before they were transformed. The pre-urban NPP, which represented the NPP that would exist in the absence of urban land development, was then computed under the pre-urban conditions (Imhoff et al., 2004). That is, the mean NPP of the surrounding non-urban neighborhood of an urban cell was used as a proxy to the original state of this urban cell before it was transformed. For covering the non-urban lands around some metropolis such as Beijing, Shanghai and Guangzhou in China, several neighborhoods with different radius such as 100-km, 120-km and 150-km were tested, and no significant pre-urban NPP changes were noted by using these different radiuses. Therefore, a neighborhood of 100-km radius was selected when calculating the pre-urban NPP for simplicity. In detail, the pre-urban NPP was calculated by replacing the current NPP (post-urban) of urban cells with the average post-urban NPP of non-urban cells within a 100-km radius of the urban cells corresponding to their original vegetation types in vegetation map.

In this paper, two kinds of pre-urban NPP, namely PRE-NOU and PRE-U2000 NPP, were computed based on the post-urban (POST-U2006) NPP by using the method of neighborhood proxy. The PRE-NOU NPP (NPP$_{PRE-NOU}$) refers to the NPP distributions of the original vegetation without urban land development, whereas PRE-U2000 NPP is for the urban areas in 2000 (NPP$_{PRE-U2000}$). After this, the differences between the POST-U2006 and these two pre-urban NPP (NPP$_{PRE-NOU}$ and NPP$_{PRE-U2000}$) were calculated to evaluate the impacts of urban land development on NPP for the period 2000–2006.

3.2.3. Analyses of the regional differences in NPP variations and their mechanisms

Once the POST-U2006 NPP and the difference maps were constructed, several analyses were performed to explore the regional differences and mechanisms of the NPP variations caused by urban land development. The magnitudes and proportions of the variations were counted according to the local conditions such as vegetation type, dry-wet zone and land use in China. For understanding the mechanisms of these variations, the distributions of LST and rainfall in Yangtze River Delta (YRD) and Pearl River Delta (PRD) were investigated for urban lands and vegetation, respectively. The differences of LST and rainfall between urban lands and non-urban areas were also calculated for these two regions.

4. Results and discussions

4.1. Land-use/cover changes caused by urban land development

In the past decades, urban lands have increasingly expanded in the process of the rapid economic development in China. Fig. 1 shows the spatial distributions of the land use/covers across this country in 2006. According to our calculations, urban areas in this period covered about 44,431 km^2 and occupied 0.468% of total land areas of the whole country. In addition, urban land development in China was primarily concentrated in the mid-eastern and southeast coastal areas with some of the most productive croplands.
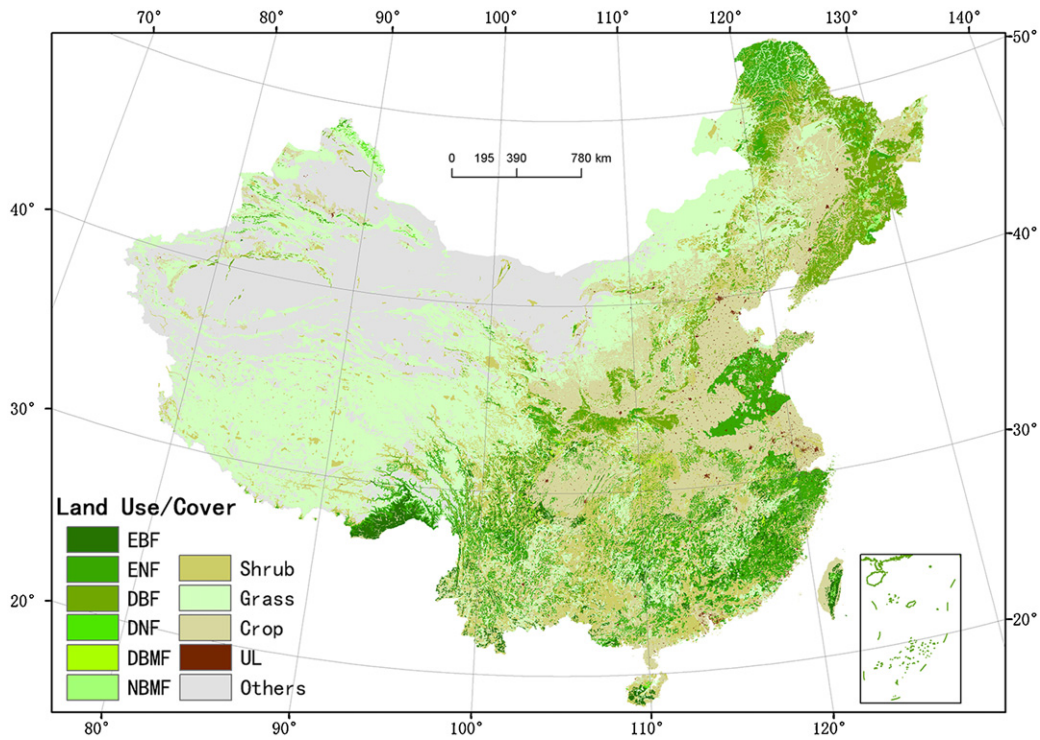
Fig. 1. Spatial distributions of the land use/cover under post-urban conditions in China. Refer to Table 1 for the legend details.

Many croplands were transformed to urban areas, accounting for 74% (more than 32,664 km^2) of total urban areas of this country (Fig. 2). This implies that urban expansions have caused massive losses of croplands in China. The similar results are also found in Liu et al. (2005)'s studies.

As shown in Fig. 2, the proportions of urban areas converted from various natural vegetation types exhibited large differences in China. Aside from croplands, evergreen needleleaf forests contributed to urban land development as well. This was primarily

associated with the wide distributions of this vegetation type across the country. In addition, shrubland and grassland occupied a large proportion of all the transformed urban areas. These results show that urban land development, one of the most dramatic landscape changes across China in recent years, reduced the amounts of cultivated lands, forest and so on. Moreover, this reduction could affect the NPP and even food security of the whole country (Liu et al., 2005; Gong, 2011). However, other forms of land use/cover changes (e.g., forest to croplands) might affect the NPP as well.
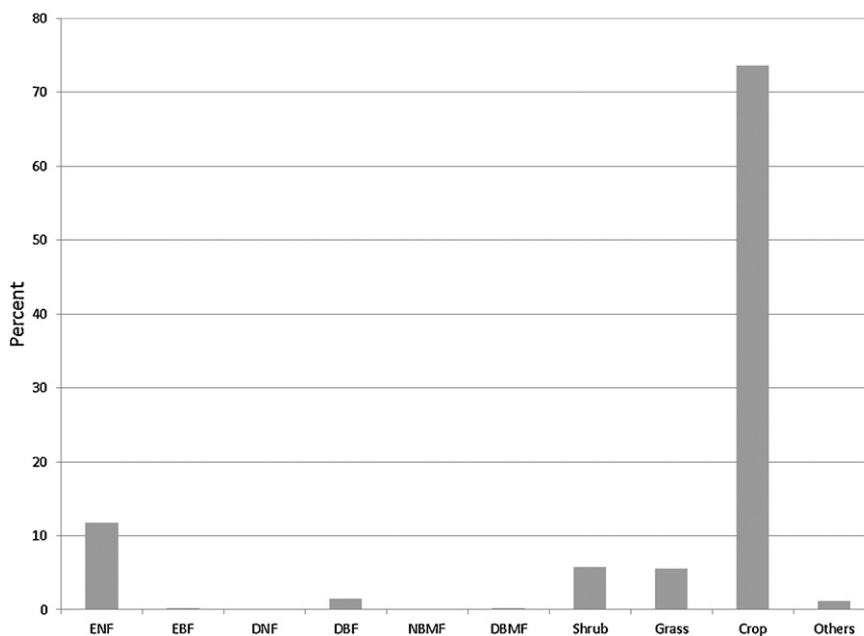

Fig. 2. Percentages of the land use/cover change conversion from original vegetation to urban lands across China. Refer to Table 1 for the legend details.
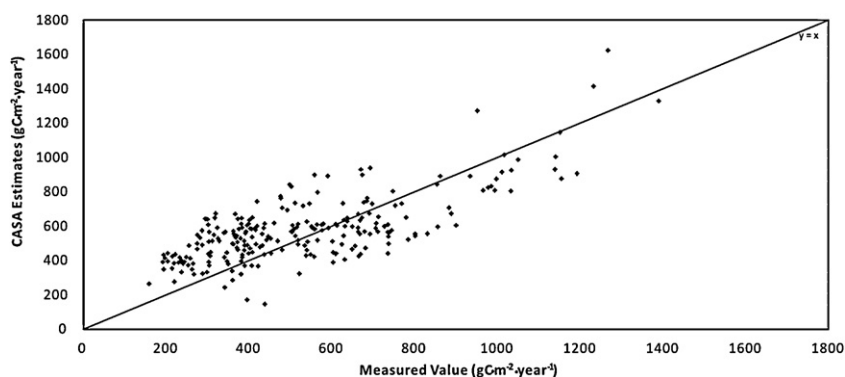
Fig. 3. Relationships between observed net primary productivity (NPP) and simulated NPP ($r = 0.733$, $P < 0.001$, $n = 248$).

4.2. The POST-U2006 NPP under current climate conditions

4.2.1. Estimates of maximum light use efficiency

In this paper, the maximum light use efficiency (ε_{max}) was obtained by calibrating the CASA model. Our simulated ε_{max} of several typical vegetation types in China are listed in Table 1. They vary between 0.348 g C MJ^{-1} for shrub and 0.630 g C MJ^{-1} for evergreen broadleaf forest. These values are mostly within the values of 0.389 g C MJ^{-1} proposed by Potter et al. (1993) and the simulated values from BIOME-BGC model (Running et al., 2000). In addition, these ε_{max} values are a little lower than the results of Zhu et al. (2006). This may be attributed to the larger conversion factor of 0.475 from dry matter (DM) to carbon content (g C m^{-2} year^{-1}) they used.

4.2.2. Validation of the NPP calculations

In this paper, the CASA model was employed to simulate the temporal and spatial distributions of the NPP in China. Verification of the reliability for the application of this model in the region is essential for the use of 1-km MODIS NDVI dataset. Therefore, we selected the plot sites with the same vegetation types as those of the vegetation map used in our study from Luo (1996)'s investigation. A correlation analysis between the NPP calculated from the CASA and the site-based data was performed for the validation of our simulated results. As shown in Fig. 3, a good coincidence can be found between the estimated NPP and the observation-based data ($r = 0.733$, $P < 0.001$, $n = 248$). This indicates that the CASA is applicable to the modeling of the NPP across China. In addition, a comparison was conducted between our calculated NPP and other published summaries of NPP studies (Table 2). The results indicate that our simulated annual NPP of China is within the reported values ranging from 1.95 to 6.13 Pg C year^{-1} (1 Pg C = 10^{15} g C). According to our study, the POST-U2006 NPP in China is 2.54 Pg C year^{-1}, closing to Sun and Zhu (2000)'s results (2.645 Pg C year^{-1}). The estimate of NPP in China from Piao et al. (2001) was 1.95 Pg C year^{-1} in 1997, which is slightly lower than our estimate because of the use of a smaller ε_{max} (0.389 g C MJ^{-1}) for all types of vegetation in China (Zhu et al., 2006). In contrast, Chen et al. (2001)'s estimate is much larger. This was probably caused by the poor quality of the data they employed (Zhu et al., 2007).

4.2.3. Spatial distributions of POST-U2006 NPP

The POST-U2006 NPP in China, which decreased markedly from southeast to northwest, showed an obvious geographical heterogeneity in both the amounts and the spatial distributions (Fig. 4). In terms of the causes, the heat energy from solar radiation not only affects the vegetation NPP directly, but also influences the NPP by its correspondence with water resource. Thus, the difference of NPP was associated with the uneven distributions of the water and heat energy in China. As for individual grid cell, annual NPP ranged from the values less than 10 g C m^{-2} year^{-1} in the desert regions in northwest China to the values greater than 1600 g C m^{-2} year^{-1} in evergreen broadleaf forests in southeast China. For further elucidating the spatial heterogeneity of the NPP between urban and non-urban areas, average NPP was calculated for the three regions that span much of the climate conditions: humid, semi-humid and semi-arid, and arid regions (Fig. 5). The selection of this dry-wet schema was roughly based on the work of Huang (1958) and the committee on natural division of the Chinese Academy of Sciences (1959), followed by a recombination of these climate zones. Since then, a comparative analysis of the monthly and annual NPP was performed between urban and non-urban areas for these three regions (Fig. 6).

The amounts of the POST-U2006 NPP for urban and non-urban areas in the humid (region I), semi-humid/semi-arid (region II) and arid regions (region III) are shown in Fig. 6. It indicates that temperature and precipitation might be the main drivers of the terrestrial NPP at the national scale. Generally, in region I with abundant water and heat, photosynthetic carbon fixation was high in both the urban and non-urban areas (270 g C m^{-2} year^{-1} and 516 g C m^{-2} year^{-1}, respectively) under the influences of the southeast and southwest monsoons. However, in the regions with less precipitation (region III), the annual NPP was 78 g C m^{-2} year^{-1} for urban areas, and 22 g C m^{-2} year^{-1} for non-urban areas. Thus, the mean NPP of non-urban areas was much lower than that of urban areas. This might be related to two factors: firstly, the NPP was very low in the non-urban areas of this region, and some of which even closed to zero, such as in Taklimakan Desert. Besides, urban areas in this region, which have good irrigation conditions, were extremely small, only about 1464 km^2. In such situation, natural conditions (e.g., water and heat) of urban areas were relatively suitable for the stable NPP in comparison with the non-urban areas. In region II, the NPP values of urban and non-urban areas (184 g C m^{-2} year^{-1} and 214 g C m^{-2} year^{-1}, respectively) were within the range of regions I and III because of the transitional climate conditions in this region.

Table 2
Comparisons of our simulated NPP with the results of past studies.

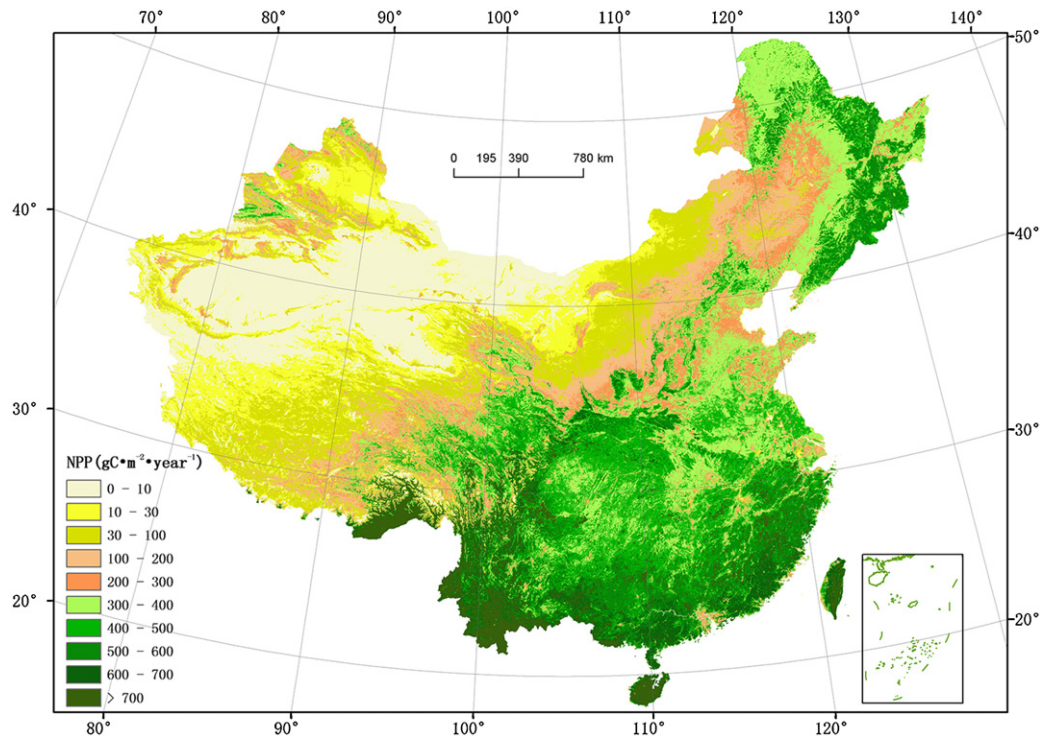|	NPP (PgC·year^{-1})	Data period	Key references
1	2.645	1992–1993	Sun and Zhu (2000)
2	1.95	1997	Piao et al. (2001)
3	6.13	1990	Chen et al. (2001)
4	3.12	1989–1993	Zhu et al. (2007)
5	2.235	2001	Feng et al. (2007)
6	2.54	2001–2010	This study

Fig. 4. Spatial distributions of POST-U2006 NPP under post-urban conditions in China.

4.2.4. Seasonal dynamics of the POST-U2006 NPP

Monthly variations of the POST-U2006 NPP were analyzed to reveal the seasonal dynamics of the terrestrial carbon cycle in China. These were accomplished by calculating the NPP differences between urban and non-urban areas for each month. Figs. 7–9 show the seasonal trends of the monthly NPP in humid, semi-humid/semi-arid and arid regions. As illustrated, the mean NPP across China shows obvious seasonal dynamics between urban and non-urban areas in all the three regions. Near-zero NPP values could be found in winter (December to February) because of the low temperature and rare precipitation. The mean NPP then exhibited a continuous increase from spring (March to May) to summer (June to July), and reached a maximum value in July. This trend might be explained by the increasing heat and precipitation during the
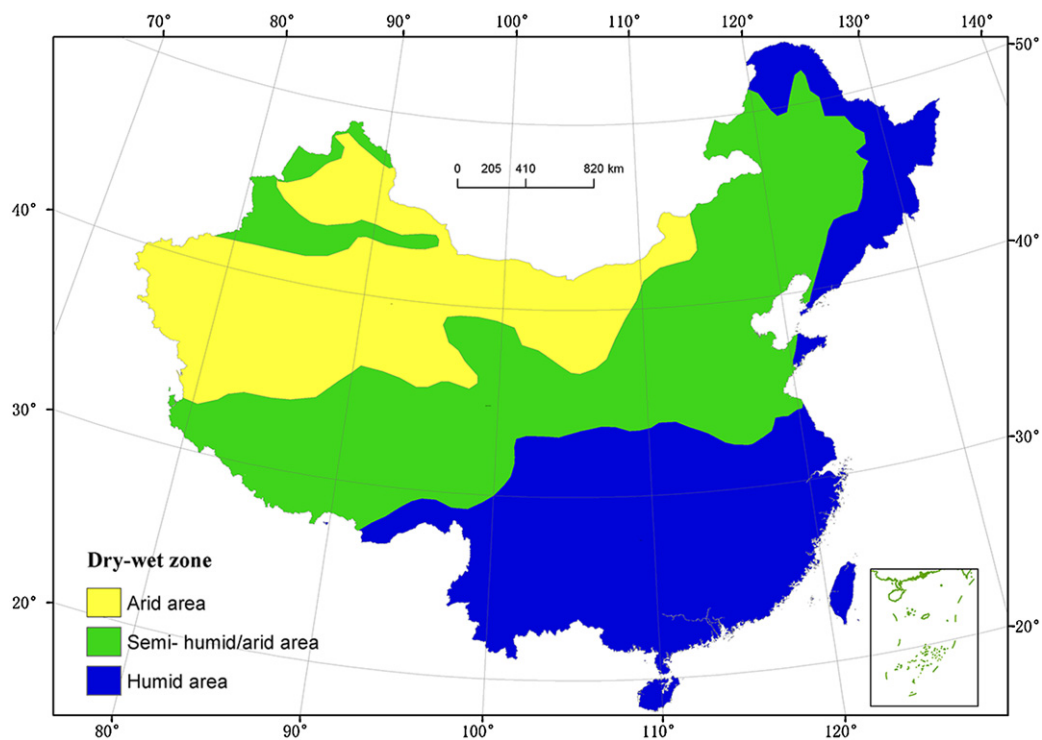

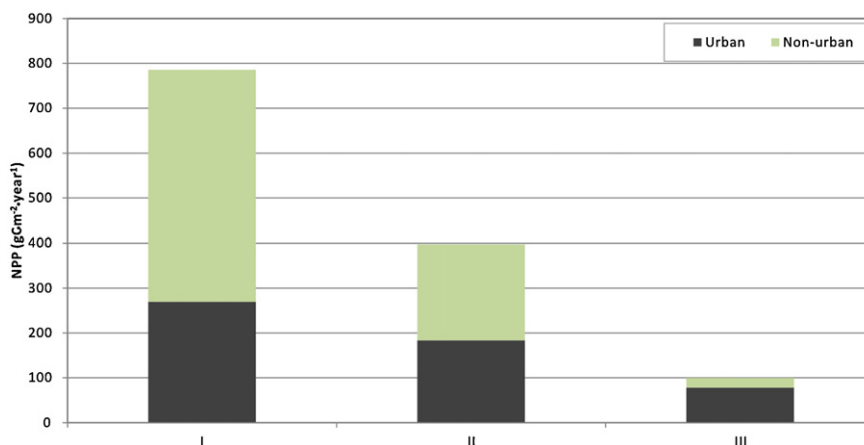**Fig. 5.** Spatial distribution of the dry-wet zones in China.

Fig. 6. Comparisons of POST-U2006 NPP for urban and non-urban areas in regions I, II and III. I: Humid area; II: semi-humid and semi-arid area; III: arid area.

growing season in this region. However, the NPP were reduced in autumn (September to November) and winter (December to February), due to the decline of both the temperature and precipitation.

In region I, which covers most of the monsoon regions in China, the mean NPP was lower in urban areas than non-urban areas during the whole year (Fig. 7a). That is, urban land development reduced the vegetation NPP even under favorable climate conditions, mainly by replacing natural vegetation with impervious surfaces. Conversely, human-sponsored resource augmentations (e.g., management practices, irrigation and fertilization) did not have dominant effects on the NPP in urban areas, compared with the reduction of vegetation cover. As shown in Fig. 7a and b, when the mean NPP peaked in July, the losses of NPP from urban land development reached its maximal value as well. This result implies that urban land development had generally negative effects on NPP.
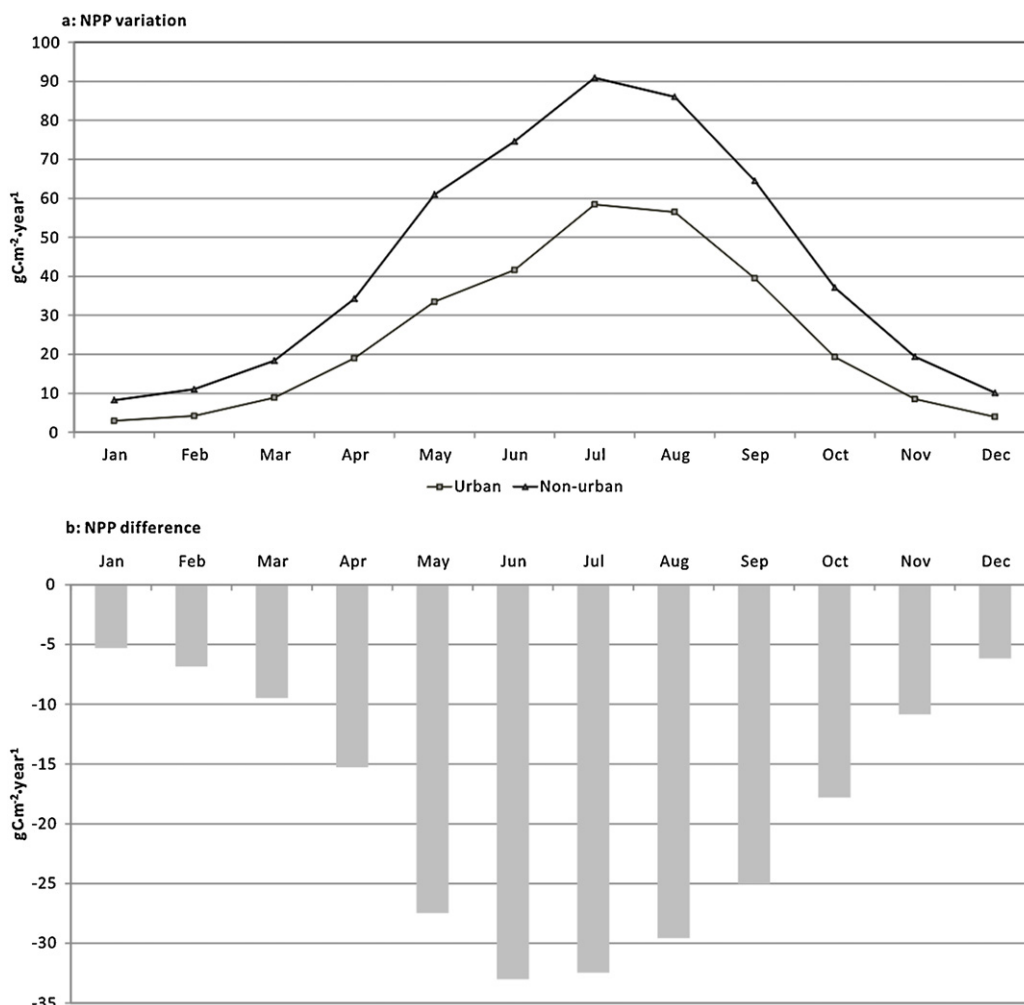

Fig. 7. Seasonal dynamics of the POST-U2006 NPP in region I. Refer to Fig. 6 for the region details.
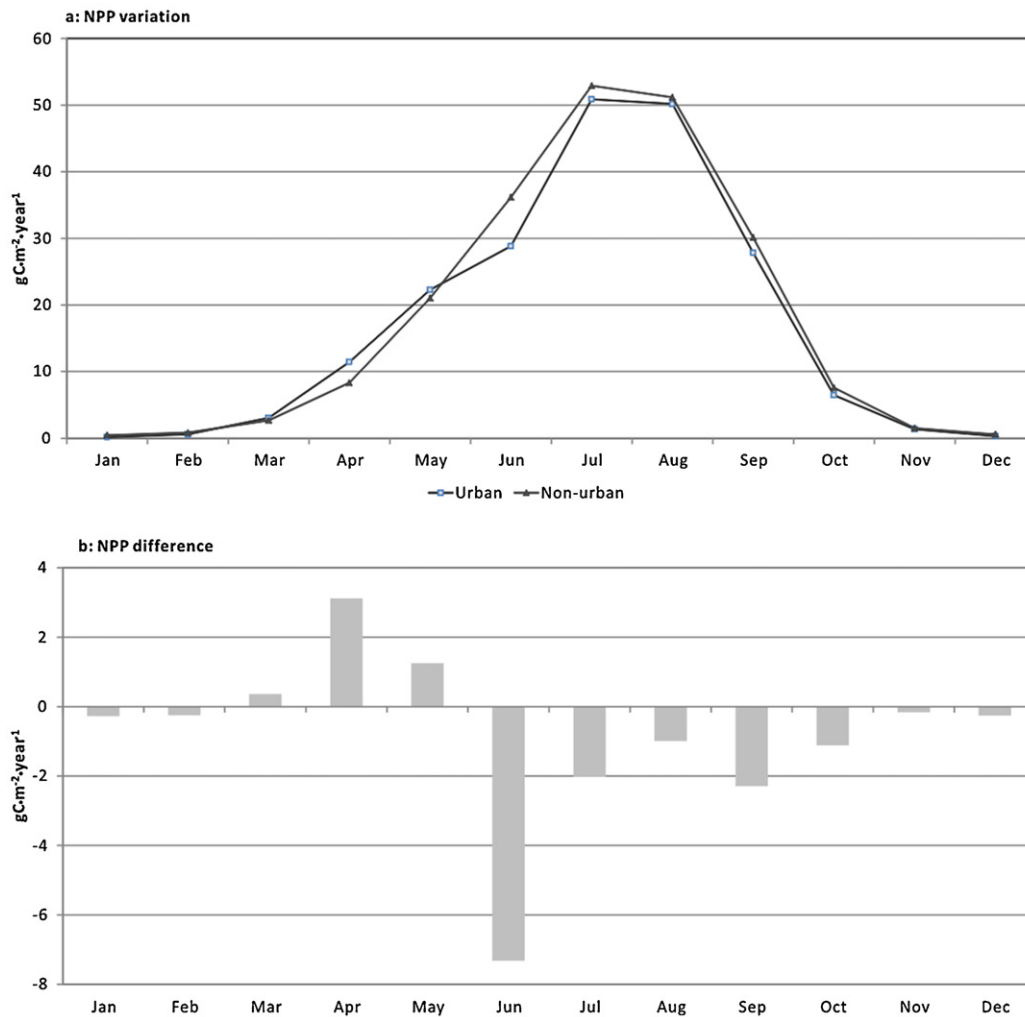
Fig. 8. The same details as Fig. 7, but for region II.

It might lead to some net losses even under favorable temperature and precipitation.

In region II with a semi-humid and semi-arid climate, the monthly NPP in urban and non-urban areas were both lower than the values in region I during most of the periods (Fig. 8a). Urban land development exhibited as net losses of NPP in the growing season (Fig. 8b). This was possibly caused by the insufficient precipitation and heat in this period.

In region III with an arid climate, some of urban areas exhibited higher NPP than non-urban areas (Fig. 9a). This indicates that urban land development dramatically influenced the seasonal variations of NPP in this region. These high NPP might be caused by an introduction of faster growing exotics instead of native plant species facilitated by ecosystem alterations (Buyantuyev and Wu, 2009), resource augmentations (such as management practices, irrigation and fertilization) and so on. Moreover, since the special location of non-monsoon zone, melted water from glacial/snow has crucial influences on the discharge regulation of inland rivers in this region (Wang and Cheng, 2000). Consequently, temperature has substantial effects on the water supply, and hence on the vegetation activity. Thus, this factor was responsible for the net increase of NPP during the warm seasons (April to October) in this region (Fig. 9b).

Take the country as a whole, an obvious temporal and spatial heterogeneity of the NPP variations could be observed in both the urban and non-urban areas. The dominant factors of this heterogeneity exhibited dramatic regional differences. In the humid region of southeast China, rainfall played an important role in the NPP, in comparison with the crucial influences of temperature and water in the northwest arid region.

4.3. Variations of NPP caused by urban land development

Since 1978, China has experienced rapid and unprecedented urbanization, accompanied by massive urban land development. This exhibits dramatic effects on the NPP at different scales. For understanding the effects of urban land development on NPP, we focused on the conversion from various types of vegetation to urban lands. Two kinds of pre-urban NPP ($NPP_{PRE-NOU}$ and $NPP_{PRE-U2000}$) were simulated. The differences between the post-urban and pre-urban NPP ($NPP_{POST-U2006}-NPP_{PRE-NOU}$, $NPP_{POST-U2006}-NPP_{PRE-U2000}$) were analyzed as well.

As shown in Fig. 10a–d, urban land development in China underwent substantial NPP losses, and mostly concentrated in and around some of large urban centers, with a maximal value of more than $500 \, g \, C \, m^{-2} \, year^{-1}$. However, this type of land use might be associated with a slight increase of NPP. This phenomenon mainly occurred around some of the urban areas that have experienced rapid urbanization, including YRD and PRD. For exploring the mechanics of the NPP variations, we investigated the effects of Urban Rain Island (URI) and Urban Rain Island (URI) in the regions of YRD and PRD for the period 2001–2010. Table 3 indicates that
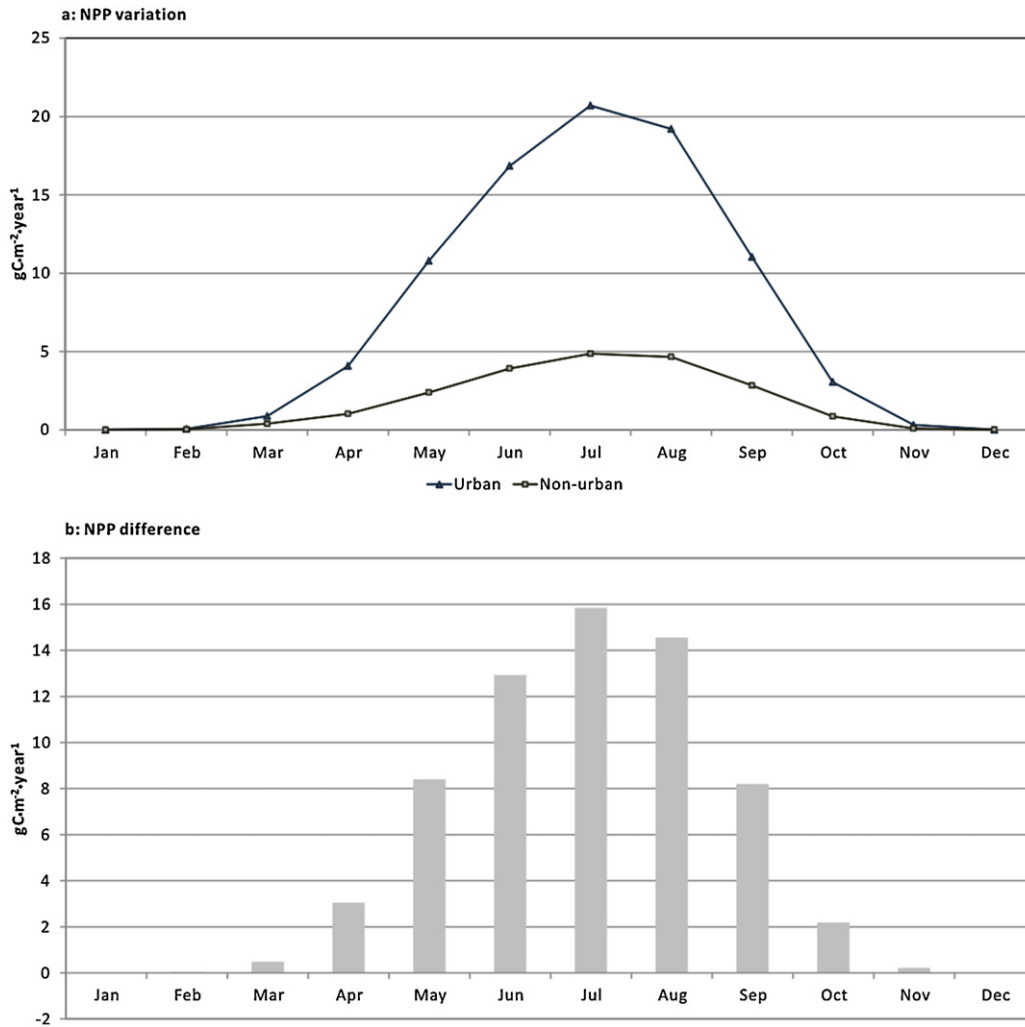
Fig. 9. The same details as Fig. 7, but for region III.

remarkable effects of UHI occurred in PRD in this period. The URI in YRD was just the same way as in PRD. However, average LST of the urban lands in YRD was slight higher than the vegetation, so was the rainfall in PRD. These indicate that the increases of NPP might be correlated with the effects of UHI and URI caused by urban land development (Chen et al., 2006; Ding et al., 2010). Besides these, other factors, including the resource augmentations (e.g., management practices, irrigation and fertilization), an introduction of faster growing exotics instead of native plant species (Buyantuyev and Wu, 2009), might also contribute to this increase. In addition, some of the arid regions in northwest China exhibited an increase as well (Figs. 10 and 11). In these regions, the increase of NPP was probably associated with the resource augmentations and the influences of some introduced plant species with higher productivity facilitated by ecosystem alterations (Buyantuyev and Wu, 2009).

In terms of the difference between $NPP_{POST-U2006}$ and $NPP_{PRE-NOU}$, the conversion from various types of vegetation to urban areas resulted in losses of 5.27×10^{-3} Pg C year^{-1}, approximately 0.21% of total POST-U2006 NPP. Especially, these losses might account for about 4.97% of annual vegetation carbon sinks and 0.80% of annual carbon emissions from the consumption of fossil fuel in this country (Fang et al., 2007). As to the difference between $NPP_{POST-U2006}$ and $NPP_{PRE-U2000}$, the losses reached 3.08×10^{-3} Pg C year^{-1}. This indicates a reduction of NPP at an accelerating rate of 0.31×10^{-3} Pg C year^{-1}, approximately 5.88% of the annual reduction in China during the period of 2000–2006. Thus, a proper regulation of urban land development is in urgent need for reducing the negative effects on carbon cycle at regional and even global scales.

In addition, the difference maps between POST-U2006 NPP and PRE-NOU/PRE-U2000 NPP were extracted for the humid (region I),

Table 3

Land surface temperature (LST), rainfall as well as the difference between them in the regions of Yangtze River Delta (YRD) and Pearl River Delta (PRD) for the period 2001–2010.

Region	LST(K)			Rainfall (mm year^{-1})		
	UL	VEG	UL-VEG	UL	VEG	UL-VEG
YRD	289.1	288.1	1.0	1214.0	1170.0	44.0
PRD	305.4	302.2	3.2	1912.9	1898.6	14.3

VEG represents vegetation areas; UL represents urban lands; VEG-UL represents the difference of average LST/annual total rainfall between urban areas and vegetation.
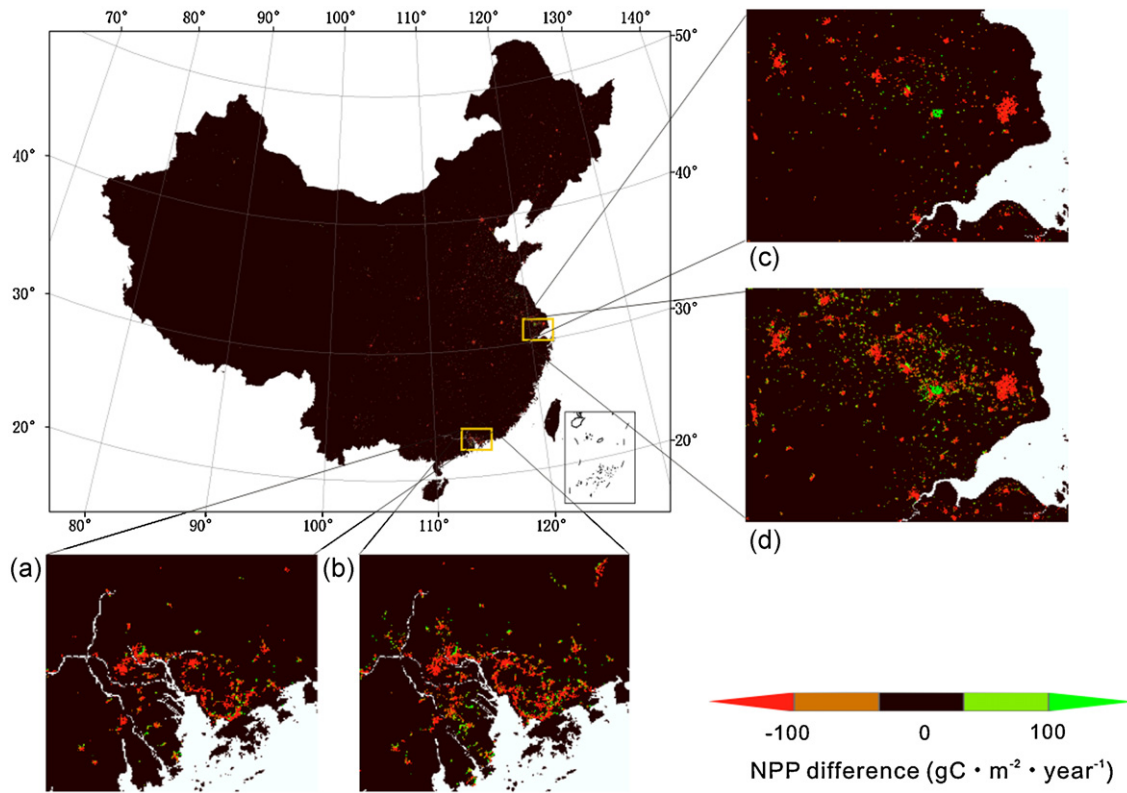
Fig. 10. Spatial distributions of the NPP variations caused by urban land development. These were calculated as: (a) difference between the POST-U2006 and PRE-U2000 NPP in Pearl River Delta; (b) difference between the POST-U2006 and PRE-NOU NPP in Pearl River Delta; (c) the same details as a, but for Yangtze River Delta; (d) the same details as b, but for Yangtze River Delta.

semi-humid/semi-arid (region II) and arid regions (region III). As illustrated by Fig. 11, the NPP variations were mostly characterized by net carbon losses in all these regions. With the reductions of precipitation from the southeast coastline (region I) to western inland areas (region III) in China, the losses of NPP showed an obvious decrease due to the water insufficiency. However, a slight increase of NPP could also be noted, especially in some of arid regions. This was probably caused by the resource augmentations and the influences of some introduced plant species with higher productivity.

The NPP variations from urban land development were also investigated according to their corresponding original vegetation types (Fig. 12). According to our calculations of the differences between POST-U2006 and PRE-U2000 NPP, the conversions from croplands resulted in losses of 2.37 Tg C (1 Tg C = 10^{12} g C). However, the NPP losses based on the differences between POST-U2006 and PRE-NOU NPP reached 3.99 Tg C, approximately 75% of total NPP reduction. Such losses might be associated with the massive conversion from croplands to urban land development (Li, 1998; Weng, 2002; Liu et al., 2005), which exhibits crucial influences on the food security of the whole country (Liu et al., 2005; Gong, 2011). Therefore, it is challenging for further studies to model the temporal and spatial evolutions of both cropland losses and their impacts on terrestrial NPP.
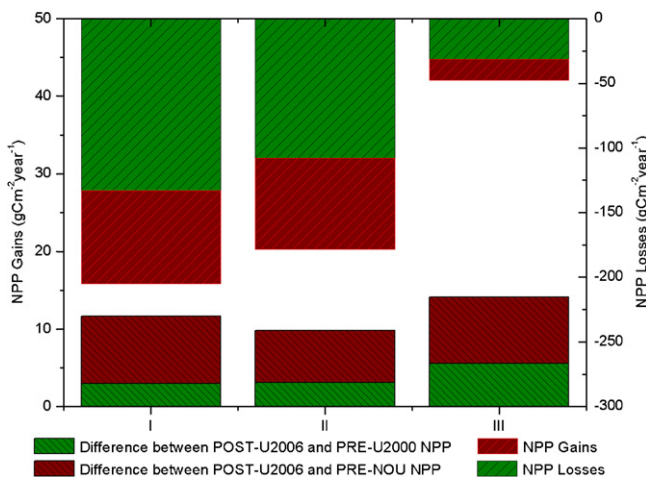

Fig. 11. NPP gains/losses caused by urban land development in regions I, II and III. Refer to Fig. 6 for individual region details.
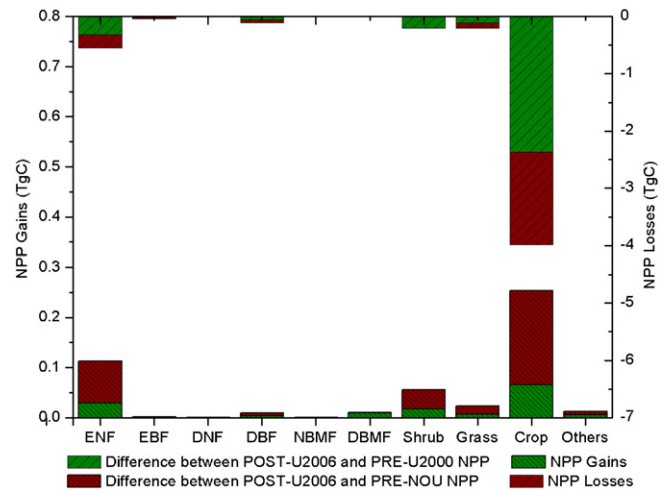

Fig. 12. NPP gains/losses from urban land development counted by its original vegetation. Refer to Table 1 for legend details.

5. Conclusions

Urban land development, which exhibits marked effects on the terrestrial carbon cycle, has been one of the most important types of land use/cover changes in China in recent years. With the growing scientific and political interest in the effects of the terrestrial carbon cycle on global climate changes, it is essential to understand the impacts of urban land development on the carbon cycle, especially the NPP. In this study, temporal and spatial variations of the terrestrial NPP induced by urban land development in China, as well as their mechanisms were investigated by performing three NPP simulations (namely POST-U2006, PRE-NOU and PRE-U2000 NPP). A new calibration was performed by using 1-km MODIS NDVI to obtain the maximum light use efficiency for adapting the CASA on the fine-scale applications such as urban land development. The NPP variations caused by urban land development were investigated by calculating the differences between the post-urban (POST-U2006) and pre-urban (PRE-NOU and PRE-U2000) NPP in China, respectively. The overall effect was that it dramatically reduced the NPP of this country. Moreover, our findings also indicated a dramatic geographical heterogeneity in the amounts and spatial distributions between urban and non-urban areas, although it corresponded well with the local climate and land use/covers conditions. As to the difference between POST-U2006 and PRE-NOU NPP, the estimated reduction of NPP induced by urban land development in China was 5.27×10^{-3} Pg C year^{-1}, approximately 0.21% of the POST-U2006 NPP. However, the losses of NPP reached 3.08×10^{-3} Pg C year^{-1} according to the calculations of the difference between NPP$_{POST-U2006}$ and NPP$_{PRE-U2000}$. This indicated an accelerating NPP reduction of 0.31×10^{-3} Pg C year^{-1} during the period of 2000–2006. Particularly, the NPP variations that originated from what were croplands exhibited the losses of 3.99 Tg C year^{-1} (NPP$_{POST-U2006}$−NPP$_{PRE-NOU}$) and 2.37 Tg C year^{-1} (NPP$_{POST-U2006}$−NPP$_{PRE-U2000}$), accounting for about 75% and 45% of total reduction. Such decreases might be associated with the massive losses of croplands during the rapid urbanization in this country. These quantitative analyses of the NPP variations might help to constrain other factors in the process of carbon cycling, including climate change, deforestation and wildfire. In terms of spatial distributions, the losses of NPP caused by urban land development were markedly reduced along with the decrease of the NPP from southeast to northwest China. However, the NPP exhibited a slight increase around some urban areas that undergone rapid urbanization and some of arid regions. This was probably caused by the effects of UHI and URI, an introduction of faster growing exotics instead of native plant species facilitated by ecosystem alterations, various resource augmentations (e.g., management practices, irrigation and fertilization), and so on.

During the past few decades, the process of urbanization is accelerating at faster rates than before all over the world, accompanied with a rapid expansion of urban land development (Angel et al., 2005; Davies et al., 2011). Although land use/cover changes (especially urban land development) have been well modeled (Verburg et al., 2002; Li et al., 2011a), there are still very limited studies concerning the impacts of urban expansion on the terrestrial NPP. This paper quantitatively analyzed the urban land development and its effects on terrestrial NPP in China by using one of the important satellite-based models. However, it is essential to simulate the spatial and temporal evolutions of land use change in the near future, as well as their effects on NPP. Coupling some of process-based NPP models (Cramer et al., 1999), instead of satellite-based models, with the urban dynamic models such as CLUE-S (Verburg et al., 2002), ANN-CA (Li and Yeh, 2002) and GeoSOS (Li et al., 2011a,b) is a challenging aspect under the condition of global climate changes. In our future studies, these works need to be further explored for the country that experiencing fast urbanization.

References

Alberti, M., 2005. The effects of urban patterns on ecosystem function. Int. Reg. Sci. Rev. 28, p168.
Angel, S., Sheppard, S.C., Civco, D.L., Buckley, R., Chabaeva, A., Gitlin, L., Kraley, A., Parent, J., Perlin, M., 2005. The Dynamics of Global Urban Expansion, vol. 1. Transport and Urban Development Department, The World Bank, p. 3.
Buyantuyev, A., Wu, J., 2009. Urbanization alters spatiotemporal patterns of ecosystem primary production: a case study of the Phoenix metropolitan region, USA. J. Arid Environ. 73, 512–520.
Chen, L.J., Liu, G.H., Fen, X.F., 2001. Estimation of net primary productivity of terrestrial vegetation in china by remote sensing. Acta Bot. Sin. 43, 1191–1198.
Chen, X.L., Zhao, H.M., Li, P.X., Yin, Z.Y., 2006. Remote sensing image-based analysis of the relationship between urban heat island and land use/cover changes. Remote Sens. Environ. 104, 133–146.
Committee on Natural Division Sciences, 1959. Climatic Regionalization of China. Science Press, Beijing.
Cramer, W., Kicklighter, D.W., Bondeau, A., Iii, B.M., Churkina, G., Nemry, B., Ruimy, A., Schloss, A.L., 1999. Comparing global models of terrestrial net primary productivity (NPP): overview and key results. Glob. Change Biol. 5, 1–15.
Davies, Z.G., Edmondson, J.L., Heinemeyer, A., Leake, J.R., Gaston, K.J., 2011. Mapping an urban ecosystem service: quantifying above-ground carbon storage at a city-wide scale. J. Appl. Ecol., 1–10.
DeFries, R.S., Houghton, R.A., Hansen, M.C., Field, C.B., Skole, D., Townshend, J., 2002. Carbon emissions from tropical deforestation and regrowth based on satellite observations for the 1980s and 1990s. Proc. Natl. Acad. Sci. U.S.A. 99, 14256.
Ding, J., Xu, Y., Pan, G., 2010. Effect of urbanization on regional precipitation in suzhou-wuxi-changzhou area. Resour. Environ. Yangtze Basin 19, 873–877.
Editorial Board of Vegetation Map of China, 2001. Vegetation Atlas of China (1:1,000,000). Science Press, Beijing.
Fang, J.Y., Guo, Z.D., Piao, S.L., Chen, A.P., 2007. Terrestrial vegetation carbon sinks in China, 1981–2000. Sci. China Ser. D: Earth Sci. 50, 1341–1350.
Feng, X., Liu, G., Chen, J.M., Chen, M., Liu, J., Ju, W.M., Sun, R., Zhou, W., 2007. Net primary productivity of China's terrestrial ecosystems from a process model driven by remote sensing. J. Environ. Manage. 85, 563–573.
Field, C.B., Randerson, J.T., Malmstr, C.M., 1995. Global net primary production: combining ecology and remote sensing. Remote Sens. Environ. 51, 74–88.
Freddy, N., Harrij, V.V., Luc, V., 2008. Harmonized World Soil Database. Food and Agriculture Organization of the United Nations.
Goerner, A., Reichstein, M., Tomelleri, E., Hanan, N., Rambal, S., Papale, D., Dragoni, D., Schmullius, C., 2011. Remote sensing of ecosystem light use efficiency with MODIS-based PRI. Biogeosciences 8, 189–202.
Gong, P., 2011. China needs no foreign help to feed itself. Nature, 474.
Gregg, J.W., Jones, C.G., Dawson, T.E., 2003. Urbanization effects on tree growth in the vicinity of New York City. Nature 424, 183–187.
Grimm, N.B., Faeth, S.H., Golubiewski, N.E., Redman, C.L., Wu, J., Bai, X., Briggs, J.M., 2008. Global change and the ecology of cities. Science 319, p756.
Hilker, T., Hall, F.G., Coops, N.C., Lyapustin, A., Wang, Y., Nesic, Z., Grant, N., Black, T.A., Wulder, M.A., Kljun, N., 2010. Remote sensing of photosynthetic light-use efficiency across two forested biomes: spatial scaling. Remote Sens. Environ. 114, 2863–2874.
Huang, B.W., 1958. A preliminary scheme for comprehensive physical regionalization in China. Acta Geogr. Sin. 24, 348–365.
Huang, Y., Sun, W., 2006. Changes in topsoil organic carbon of croplands in mainland China over the last two decades. Chin. Sci. Bull. 51, 1785–1803.
Imhoff, M.L., Bounoua, L., DeFries, R., Lawrence, W.T., Stutzer, D., Tucker, C.J., Ricketts, T., 2004. The consequences of urban land transformation on net primary productivity in the United States. Remote Sens. Environ. 89, 434–443.
Inoue, Y., Peñuelas, J., 2006. Relationship between light use efficiency and photochemical reflectance index in soybean leaves as affected by soil water content. Int. J. Remote Sens. 27, 5109–5114.
Jin, Z., Qi, Y.C., Dong, Y.S., 2007. Storage of biomass and net primary productivity in desert shrubland of *Artemisia ordosica* on Ordos Plateau of Inner Mongolia, China. J. Forestry Res. 18, 298–300.
Jing, F., 2009. Application of 3S technology to the updating survey of land. In: 2009 International Conference on Environmental Science and Information Application Technology, IEEE.
Kaye, J.P., McCulley, R.L., Burke, I.C., 2005. Carbon fluxes, nitrogen cycling, and soil microbial communities in adjacent urban, native and agricultural ecosystems. Glob. Change Biol. 11, 575–587.
Li, X., Chen, Y., Liu, X., Li, D., He, J., 2011a. Concepts, methodologies, and tools of an integrated geographical simulation and optimization system. Int. J. Geogr. Inf. Sci. 25, 633–655.

Li, X., Shi, X., He, J., Liu, X., 2011b. Coupling simulation and optimization to solve planning problems in a fast-developing area. Ann. Assoc. Am. Geographers 99999, p1.

Li, X., Yeh, A.G.O., 2002. Neural-network-based cellular automata for simulating multiple land use changes using GIS. Int. J. Geogr. Inf. Sci. 16, 323–343.

Li, X., 1998. Measurement of rapid agricultural land loss in the Pearl River Delta with the integration of remote sensing and GIS. Environ. Plan. B: Plan. Des. 25, 447–461.

Liu, J., Liu, M., Tian, H., Zhuang, D., Zhang, Z., Zhang, W., Tang, X., Deng, X., 2005. Spatial and temporal patterns of China's cropland during 1990–2000: an analysis based on Landsat TM data. Remote Sens. Environ. 98, 442–456.

Lobell, D.B., Hicke, J.A., Asner, G.P., Field, C.B., Tucker, C.J., Los, S.O., 2002. Satellite estimates of productivity and light use efficiency in United States agriculture, 1982–98. Glob. Change Biol. 8, 722–735.

Lu, D., Xu, X., Tian, H., Moran, E., Zhao, M., Running, S.W., 2010. The effects of urbanization on net primary productivity in southeast China. Environ. Manage. 46, 404–410.

Luo, T.X., 1996. Patterns of net primary productivity for Chinese major forest types and its mathematical models. Ph.D. Thesis. Chinese Academy of Sciences, pp. 45–170.

Milesi, C., Elvidge, C.D., Nemani, R.R., Running, S.W., 2003. Assessing the impact of urban land development on net primary productivity in the southeastern United States. Remote Sens. Environ. 86, 401–410.

Monteith, J.L., 1972. Solar radiation and productivity in tropical ecosystems. J. Appl. Ecol. 9, 747–766.

Myneni, R.B., Dong, J., Tucker, C.J., Kaufmann, R.K., Kauppi, P.E., Liski, J., Zhou, L., Alexeyev, V., Hughes, M.K., 2001. A large carbon sink in the woody biomass of northern forests. Proc. Natl. Acad. Sci. U.S.A. 98, p14784.

Ni, J., 2003. Net primary productivity in forests of China: scaling-up of national inventory data and comparison with model predictions. Forest Ecol. Manage. 176, 485–495.

Ni, J., 2004. Estimating net primary productivity of grasslands from field biomass measurements in temperate northern China. Plant Ecol. 174, 217–234.

Nichol, C.J., Huemmrich, K.F., Black, T.A., Jarvis, P.G., Walthall, C.L., Grace, J., 2000. Remote sensing of photosynthetic-light-use efficiency of boreal forest. Agric. Forest Meteorol. 101, 131–142.

Piao, S.L., Fang, J.Y., Guo, Q.H., 2001. Application of CASA model to the estimation of Chinese terrestrial net primary productivity. Acta Phytoecol. Sin. 25, 603–608.

Piao, S.L., Fang, J.Y., Zhu, B., Tan, K., 2005. Forest biomass carbon stocks in China over the past 2 decades: estimation based on integrated inventory and satellite data. J. Geophys. Res. – Biogeosci., 110.

Potter, C.S., Randerson, J.T., Field, C.B., Matson, P.A., Vitousek, P.M., Mooney, H.A., Klooster, S.A., 1993. Terrestrial ecosystem production: a process model based on global satellite and surface data. Glob. Biogeochem. Cycles 7, 811–841.

Propastin, P.A., Kappas, M.W., Herrmann, S.M., Tucker, C.J., 2012. Modified light use efficiency model for assessment of carbon sequestration in grasslands of Kazakhstan: combining ground biomass data and remote-sensing. Int. J. Remote Sens. 33, 1465–1487.

Running, S.W., Thornton, P.E., Nemani, R., Glassy, J.M., 2000. Global terrestrial gross and net primary productivity from the earth observing system. Methods Ecosyst. Sci., 44–57.

Russell, G., Jarvis, P.G., Monteith, J.L., 1989. Absorption of radiation by canopies and stand growth. In: Plant Canopies: Their Growth Form and Function. Cambridge University Press, Cambridge, UK.

Sun, R., Zhu, Q.J., 2000. Distribution and seasonal change of net primary productivity in China from April, 1992 to March, 1993. Acta Geogr. Sin. 55, 36–45.

Thornthwait, W.C., 1948. An approach toward rational classification of climate. Geogr. Rev. 38, 55–94.

Togtohyn, C., Ojima, D., 1996. NPP Grassland: Tumentsogt, Mongolia, 1982–1990. Oak Ridge National Laboratory Distributed Active Archive Center, Tennessee, USA.

Trusilova, K., Churkina, G., 2008. The response of the terrestrial biosphere to urbanization: land cover conversion, climate, and urban pollution. Biogeosciences 5, 1505–1515.

Verburg, P.H., Soepboer, W., Veldkamp, A., Limpiada, R., Espaldon, V., Mastura, S.S.A., 2002. Modeling the spatial dynamics of regional land use: the CLUE-S model. Environ. Manage. 30, 391–405.

Wang, G.L., Wu, B., Jia, C.L., Yang, Q.L., Sheng, Y.B., 2011. Grassland vegetation characterics of shrub-grass land in Wufeng mountain area of Ji'nan City. Bull. Soil Water Conserv. 31, 228–237.

Wang, G., Cheng, G., 2000. The characteristics of water resources and the changes of the hydrological process and environment in the arid zone of northwest China. Environ. Geol. 39, 783–790.

Wang, Y.P., Houlton, B.Z., 2009. Nitrogen constraints on terrestrial carbon uptake: implications for the global carbon-climate feedback. Geophys. Res. Lett. 36, pL24403.

Weng, Q., 2002. Land use change analysis in the Zhujiang Delta of China using satellite remote sensing GIS and stochastic modelling. J. Environ. Manage. 64, 273–284.

Wu, C., Niu, Z., Tang, Q., Huang, W., 2010. Revised photochemical reflectance index (PRI) for predicting light use efficiency of wheat in a growth cycle: validation and comparison. Int. J. Remote Sens. 31, 2911–2924.

Xu, C., Liu, M., An, S., Chen, J.M., Yan, P., 2007. Assessing the impact of urbanization on regional net primary productivity in Jiangyln County, China. J. Environ. Manage. 85, 597–606.

Yu, D., Shao, H.B., Shi, P.J., Zhu, W.Q., Pan, Y.Z., 2009. How does the conversion of land cover to urban use affect net primary productivity? A case study in Shenzhen city, China. Agric. Forest Meteorol. 149, 2054–2060.

Yu, Y.W., Hu, Z.Z., Zhang, D.G., Xu, C.L., 2000. The net primary productivity of potentilla fruticosa shrub. Acta Pratacult. Sin. 9, 33–39.

Zhu, W., Pan, Y., He, H., Yu, D., Hu, H., 2006. Simulation of maximum light use efficiency for some typical vegetation types in China. Chin. Sci. Bull. 51, 457–463.

Zhu, W.Q., Pan, Y.Z., Zhang, J.S., 2007. Estimation of net primary productivity of Chinese terrestrial vegetation based on remote sensing. J. Plant Ecol. 31, 413–424.